

Small-Angle Neutron Scattering Study of Protein Crowding in Liquid and Solid Phases: Lysozyme in Aqueous Solution, Frozen Solution, and Carbohydrate Powders

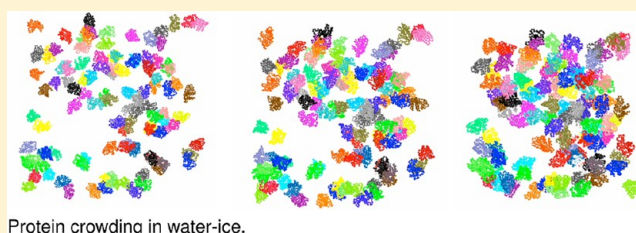
Joseph E. Curtis,^{*,†} Hirsh Nanda,[†] Sheila Khodadadi,[†] Marcus Cicerone,[†] Hyo Jin Lee,[‡] Arnold McAuley,[‡] and Susan Krueger^{*,†}

[†]NIST Center for Neutron Research, National Institute of Standards and Technology, 100 Bureau Drive, Mail Stop 6102, Gaithersburg, Maryland 20899-6102, United States

[‡]Department of Analytical and Formulation Sciences, Amgen Inc., One Amgen Center Drive, Thousand Oaks, California 91320-1799, United States

S Supporting Information

ABSTRACT: The structure, interactions, and interprotein configurations of the protein lysozyme were studied in a variety of phases. These properties have been studied under a variety of solution conditions before, during, and after freezing and after freeze-drying in the presence of glucose and trehalose. Contrast variation experiments have also been performed to determine which features of the scattering in the frozen solutions are from the protein and which are from the ice structure. Data from lysozyme at concentrations ranging from 1 to 100 mg/mL in solution and water ice with NaCl concentrations ranging from 0 to 0.4 mol/L are fit to model small-angle neutron scattering (SANS) intensity functions consisting of an ellipsoidal form factor and either a screened-Coulomb or hard-sphere structure factor. Parameters such as protein volume fraction and long dimension are followed as a function of temperature and salt concentration. The SANS results are compared to real space models of concentrated lysozyme solutions at the same volume fractions obtained from Monte Carlo simulations. A cartoon representation of the frozen lysozyme solution in 0 mol/L NaCl is presented based on the SANS and Monte Carlo results, along with those obtained from other complementary methods.



INTRODUCTION

The structure of proteins in the solid state is of interest to both the pharmaceutical and food science industries, as both industries have a need to devise ways to stabilize their products for extended periods of time without degradation. Both freezing and freeze-drying (lyophilization) are important methods used for long-term storage. However, both methods present challenges for protein stability.

As therapeutic agents, proteins provide a number of treatments for human diseases and conditions. However, the development of commercial applications is challenging due to protein stability. Proteins can be degraded chemically or physically. Chemical degradation refers to modifications involving covalent bonds, such as deamidation, oxidation, and disulfide bond shuffling, while physical degradation includes protein unfolding, undesirable adsorption to surfaces, and non-native aggregation, the latter which is particularly problematic because it is encountered routinely during refolding, purification, sterilization, shipping, and storage. Factors affecting stability include temperature, solution pH, ligands and cosolutes, salt type and concentration, preservatives, and surfactants.^{1,2} Lyophilized formulations are often developed to avoid protein degradation issues.^{3,4} Freezing is the first step of a

lyophilization process, and in many cases, especially early in the development process to manufacture a protein solution, samples are frozen to maintain biological activity.⁵ Solvent additives are often introduced into protein solutions prior to lyophilization, as they have been shown to inhibit drying-induced damage, improve the activity of proteins upon rehydration, and enhance the stability of biological systems during storage.^{5,6} A complete understanding of the spatial organization and interaction of proteins in heterogeneous frozen phases is lacking, although many interesting and promising studies have been recently reported.^{7–10} One missing aspect from these studies is the relative interprotein distance which is an important determinant in order to understand the enhancement of deleterious chemical and conformational changes that occur at increased rates in the crowded environment.

Freezing is an important preservation method used to prevent the growth of microorganisms and to slow chemical reactions, such as oxidation, to preserve the quality, nutrient

Received: May 16, 2012

Revised: July 16, 2012

Published: July 23, 2012

content, texture, flavor, and color of foods.¹¹ Therefore, the freezing process and its effects on water, proteins, lipids, carbohydrates, vitamins, and minerals in food must be well understood. Although foods are complex, their state diagram¹² exhibits similar features to those of simpler systems such as proteins in aqueous solutions. Thus, an understanding of the freezing process in more complex systems such as foods can be obtained by studying these simpler model systems. During the freezing of a typical protein solution, only a fraction of the water molecules form the crystalline ice phase, whereas the remaining water molecules and other solutes present remain in the amorphous state, forming a freeze-concentrated solution, with a water mass fraction of 30 wt %.¹³ Many proteins are known to suffer inactivation upon freezing, which can occur due to dissociation, aggregation, or other chemical mechanisms.¹⁴ Proteins can also become denatured, or unfolded, as a result of freezing.^{7–9,15} The extent of denaturation of proteins upon freezing depends on several factors including the initial pH, the protein concentration, the temperature of the frozen part of the solution, and the presence of other substances, such as salt or sugar, in the solution.¹⁴ It has been noted that NaCl can inhibit protein denaturation down to $-30\text{ }^{\circ}\text{C}$, at which point the salt likely begins to precipitate, and eventually, the freeze-concentrated liquid approaches the same composition as it would have in the absence of salt.¹⁴ Structural changes in cold-denatured proteins have been studied using fluorescence^{7,15} and nuclear magnetic resonance spectroscopy (NMR).¹⁶ In addition, protein aggregation during freeze–thawing has been investigated using ultraviolet (UV) spectroscopy.¹⁷ However, in general, structural studies of proteins in frozen solutions have been limited.

Numerous studies have been used to study biomacromolecular dynamics in hydrated powders, membranes, and cells.^{18–20} These important studies have yielded information regarding the molecular dynamics of biomacromolecules, yet they lack molecular level structural characterization. Thus, information regarding the packing and arrangement of proteins in the condensed phase is useful to the neutron spectroscopy community for both the interpretation of experimental data and the development of realistic models for molecular simulations.

Small-angle neutron scattering (SANS) probes structure and interactions on length scales from $10\text{ }\text{\AA}$ to greater than $1000\text{ }\text{\AA}$, making it a well-suited technique for the study of proteins in a variety of phases. Unlike X-rays, neutrons are sensitive to the light elements such as carbon, hydrogen, nitrogen, and oxygen that make up most proteins. Neutrons are also sensitive to different isotopes of many elements, including hydrogen. This enables the substitution of deuterium for hydrogen in the protein or aqueous solution, making it possible to determine the origin of features in the scattering curves by performing contrast variation experiments. Finally, since neutrons interact weakly with matter, making it possible to measure samples in complex environments such as cryostats.

In this work, SANS was used to directly probe the structure and interactions of the model protein, lysozyme, in aqueous solution and water ice as a function of temperature, rate of temperature change, and salt (NaCl) content. Contrast variation experiments were performed to isolate the scattering due to the protein from that due to the frozen components and the salt. The results are compared to those obtained for lysozyme in lyophilized powders in the presence of glucose and trehalose. Molecular Monte Carlo simulations were also performed on a simple model of lysozyme at protein

concentrations that were equivalent to those determined from the SANS data. The SANS and modeling results, combined with those obtained from other techniques, were used to construct a picture of the frozen state of the lysozyme solution, including the location and aggregation state of the protein.

EXPERIMENTAL METHODS

Materials. Lysozyme was purchased from Sigma and used without further purification. Certain commercial equipment, instruments, materials, suppliers, or software are identified in this paper to foster understanding. Such identification does not imply recommendation or endorsement by the National Institute of Standards and Technology, nor does it imply that the materials or equipment identified are necessarily the best available for the purpose. Lysozyme solutions for SANS experiments were prepared in 99.9% D_2O (Cambridge Isotope Laboratories, Inc.) at protein concentrations ranging from 0.5 to 150 mg/mL. Similar concentration series of solutions were prepared with 0, 0.05, 0.15, and 0.4 M NaCl added to the solution. Measured pD values were near 7 for all solutions. In addition, a series of 100 mg/mL lysozyme solutions with 0 M NaCl were prepared in differing amounts of $\text{D}_2\text{O}/\text{H}_2\text{O}$, i.e., 0, 5, 10, 20, 40, and 100 vol % D_2O , in order to perform a contrast variation experiment in the frozen state. Corresponding $\text{D}_2\text{O}/\text{H}_2\text{O}$ solutions without protein were also prepared to measure for comparison.

For measurements of protein in hydrated powders, lysozyme at $\sim 100\text{ mg/mL}$ was prepared in d_6 -glucose or partially deuterated trehalose at approximately a mass fraction of 5 wt % of glucose or trehalose in deuterium oxide (D_2O). Partially deuterated trehalose was prepared as previously described.²¹ The resulting solution was sterile filtered and filled as a 1 mL volume in partially stoppered 3 mL lyophilization glass vials. Lyophilization of the samples was conducted using a VirTis (Gardiner, NY) Genesis 12EL lyophilizer controlled by a Wizard Synoptic version 6. Shelf temperature was lowered to $-45\text{ }^{\circ}\text{C}$ over 60 min and held for 1 h. Shelf temperature was raised to $-12\text{ }^{\circ}\text{C}$ and held for 3 h and then lowered to $-45\text{ }^{\circ}\text{C}$ over 1 h where it was held for a further 2 h. Primary drying was started by lowering the chamber pressure to 13.3 Pa and raising the shelf temperature to $-10\text{ }^{\circ}\text{C}$, where it was held to $\sim 10\text{ h}$. Secondary drying was conducted by raising the shelf temperature to $25\text{ }^{\circ}\text{C}$ and held at $25\text{ }^{\circ}\text{C}$ for 12 h. Vials were stoppered under partial dry nitrogen, removed from the lyophilized, and stored at $4\text{ }^{\circ}\text{C}$ prior to analysis.

Protein Characterization. Secondary structure of lysozyme was studied using circular dichroism (CD) spectroscopy. The far-UV spectra were obtained on Jasco J-810 spectropolarimeters (Easton, MD) at room temperature from 190 to 250 nm. Lysozyme was diluted to 0.25 mg/mL in the appropriate buffer system. Protein solutions were carefully placed in a Hellma quartz cuvette (Müllheim, Germany) with a path length of 0.1 cm, and data were collected at a scan speed of 20 nm/min. All spectral data were reported as the average of a minimum of three wavelength scans, with a minimum data collection time of eight seconds per wavelength, using a 1 nm bandwidth and wavelength interval of 0.5 nm. The CD spectrum of the buffer solution was subtracted for each spectrum.

Lysozyme concentration was measured using a Hewlett-Packard UV Chemstation 8453 (Palo Alto, CA) at 280 nm. Samples were diluted with D_2O to the appropriate concentration. A Hellma quartz cuvette (Müllheim, Germany) with a 1

cm path length was used to measure UV absorbance. Samples were scanned from 200 to 400 nm. Concentration was determined using the equation concentration (mg/mL) = $(A_{280} - A_{350})/\epsilon$, where A_{280} is the absorbance at 280 nm and A_{350} is the absorbance at 350 nm, using an extinction coefficient, ϵ , of 2.65 mL mg⁻¹ cm⁻¹ at 280 nm for lysozyme.

Size exclusion high performance liquid chromatography (SE-HPLC) was performed using an Agilent 1100 (Palo Alto, CA) equipped with a quaternary pump, diode array detector, and refrigerated autosampler. Two Tosohaas G2000SWxL TSK columns, 5 μ m particle size, 7.8 mM i.d. \times 30 cm (Montgomeryville, PA), were used in series. 50 μ g of sample was injected and eluted over 30 min using 25 mM sodium phosphate, 125 mM sodium chloride, pH 6.9, as the running buffer at 0.6 mL/min. Absorbance was monitored at 215 nm and at 280 nm. Data were collected using Agilent Chemstation software.

Small-Angle Neutron Scattering. SANS measurements were performed on the 30 m SANS instruments²² at the NIST Center for Neutron Research (NCNR) in Gaithersburg, MD. The neutron wavelength, λ , was 6 \AA , with a wavelength spread, $\Delta\lambda/\lambda$, of 0.15. Scattered neutrons were detected with a 64 cm \times 64 cm two-dimensional position-sensitive detector with 128 \times 128 pixels at a resolution of 0.5 cm/pixel. The data were reduced using the IGOR program with SANS macro routines developed at the NCNR.²³ Raw counts were normalized to a common monitor count and corrected for empty cell counts, ambient room background counts, and nonuniform detector response.

Data from the samples in the liquid and frozen states were placed on an absolute scale by normalizing the scattered intensity to the incident beam flux. Finally, the data were radially averaged to produce scattered intensity, $I(q)$, versus q curves, where $q = 4\pi \sin(\theta)/\lambda$ and 2θ is the scattering angle. A sample-to-detector distance of 1.3 m was used for measurements of lysozyme in D₂O to cover the range $0.03 \text{ \AA}^{-1} \leq q \leq 0.4 \text{ \AA}^{-1}$. Scattering from the larger structures in the frozen solutions was measured using sample-to-detector distances of 13.0, 5.0, and 1.5 m in order to cover the range $0.007 \text{ \AA}^{-1} \leq q \leq 0.3 \text{ \AA}^{-1}$. The scattered intensities from the samples in the liquid state were then further corrected for buffer scattering and incoherent scattering from hydrogen in the samples. The buffer scattering could not be directly subtracted from the sample scattering in the frozen state due to the presence of additional scattering at low q . In this case, the scattering from the frozen samples were approximately corrected for background scattering by subtracting the scattering from the corresponding buffers at higher q values, where the buffer scattering was flat, and then subtracting a constant of the same magnitude from the scattering at lower q values.

Lysozyme solutions were loaded into demountable 1 or 2 mm path length titanium cells with titanium windows. Samples were measured at temperatures between 20 and -80 °C. Samples were cooled either by the "fast cooling" method by placing them, from room temperature, into an environment that was already at a freezing temperature or by a "slow cooling" method by placing them into an environment that was at room temperature and slowing lower the temperature, allowing the sample to remain at each intermediate temperature for 30 min before moving on to slowly approach the freezing temperature. For the contrast variation experiment, lysozyme was made in 0, 5, 10, 20, 40, and 100% D₂O. The

corresponding solutions without protein, but with either 0 or 0.4 M NaCl, were measured at -40 °C.

Powder samples containing *d*₆-glucose and *d*-trehalose were measured at room temperature in demountable 0 mm path length titanium cells; i.e., the path length was defined by the thickness of the powder sample, with quartz windows.

Data Analysis. Data from samples in the liquid state were fit using a model SANS intensity function

$$I(q) = n_p P(q) S'(q) \quad (1)$$

where n_p is the number density of scattering particles, $P(q)$ is the scattering form factor, which depends on the shape of the particles, and $S'(q)$ is the structure factor, which describes the interactions between particles. In particular, an ellipsoid form factor that describes the lysozyme shape was used, along with a screened Coulomb structure factor that describes a system of charged, spheroidal particles in a dielectric medium.^{24,25} This model function is part of the NCNR IGOR SANS data analysis package,²³ and curve fitting was accomplished using the nonlinear curve fitting routine within IGOR. Fitting parameters are located in Table S1 and included volume fraction, ellipsoid dimensions, charge, and dielectric constant. Data from samples in the solid state, i.e., frozen and powder, were fit in the high q region using a similar model SANS intensity function, except with a hard-sphere structure factor that describes a system of monodisperse spheroidal particles interacting through excluded volume interactions (where eq 1 is fit with $S'(q)$ using eq 9 in the Supporting Information along with $P(q)$ for an ellipsoid).²⁶ Further information can be found in the Supporting Information. Both of these model SANS intensity functions include a volume fraction parameter. When fit to the SANS data, the best-fit volume fractions can be used as input parameters for Monte Carlo simulations of lysozyme clusters in the liquid and solid states.

Contrast variation data with and without protein were normalized to a common background of 1 cm⁻¹ so that the change in scattering intensities at the lowest q values measured could be visually compared as a function of percent D₂O in the buffer. The scattering contrast, $\Delta\rho = \rho - \rho_0$, is defined as the difference between the average scattering length density of the scattering particles, ρ , and that of the buffer, ρ_0 . The contrast comes from the $P(q)$ term in eq 1, which can be written at $q = 0$ as

$$P(0) = (\Delta\rho)^2 V_p^2 \quad (2)$$

where V_p is the particle volume. When $\rho = \rho_0$, the scattering length densities of the particle and buffer are the same and $P(q) = 0$ for all q values. This is known as the contrast match point. Visual inspection of $I(q)$ vs q as a function of percent D₂O was sufficient to determine whether a contrast match point existed for the frozen buffer alone as well as the frozen buffer with protein.

Monte Carlo simulations were performed using 108 particles using a Lennard-Jones potential in the isothermal–isobaric ensemble^{27,28} using parameters that have been reported²⁹ without the inclusion of the long-range repulsion that was used to model salt effects. The coordinates of the lysozyme protein³⁰ were mapped onto the Lennard-Jones particles with random orientation for visualization purposes. The pressure was adjusted such that the system sampled the desired volume fraction to compare configurations at state points covered in the SANS experiments.

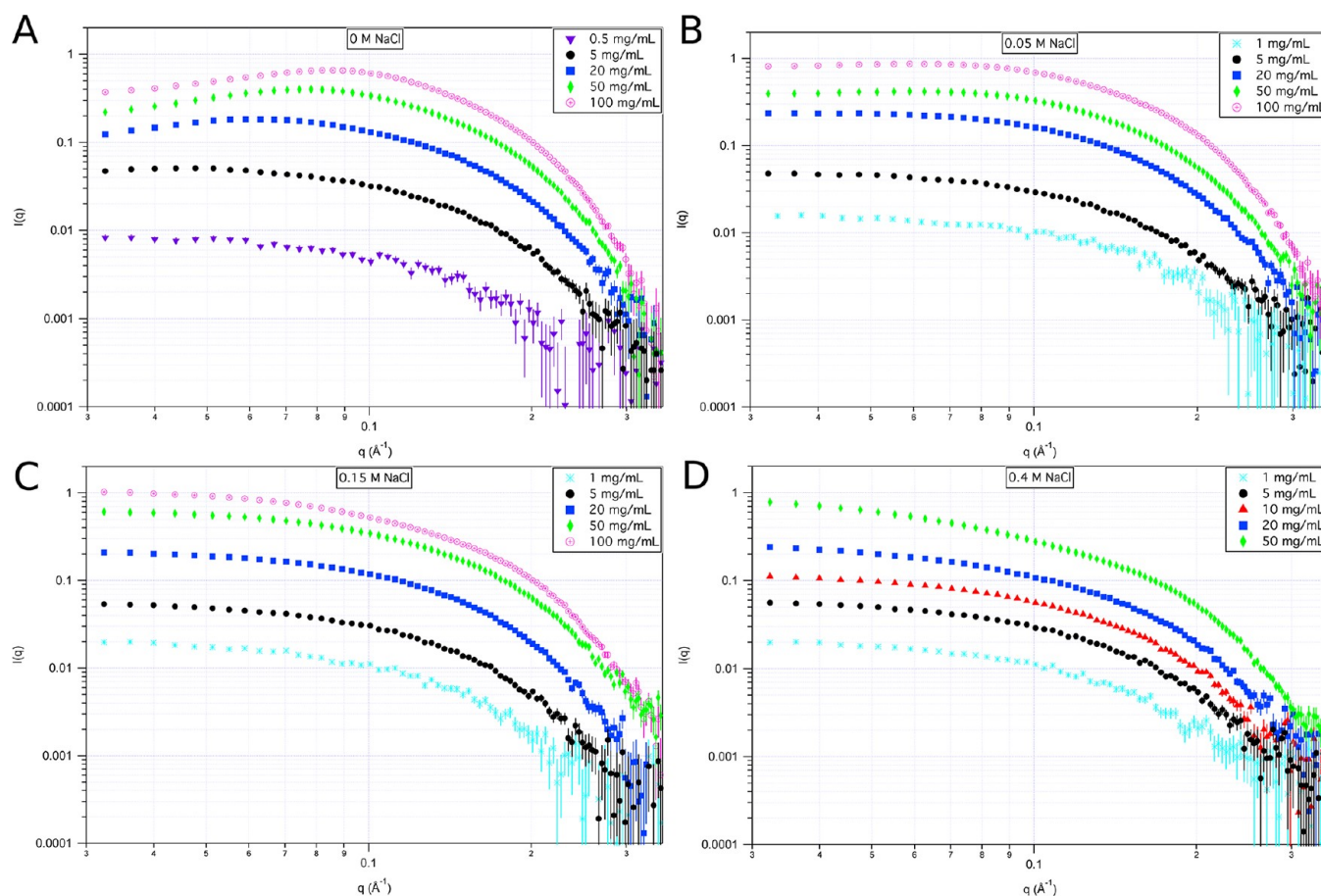


Figure 1. SANS of lysozyme in solution as a function of protein and NaCl concentration: (A) 0 M NaCl, (B) 0.05 M NaCl, (C) 0.15 M NaCl, and (D) 0.4 M NaCl.

RESULTS AND DISCUSSION

Both prior to and following SANS measurements protein containing samples were analyzed by UV and CD spectroscopy and SE-HPLC to characterize the protein content, secondary structure, and for the presence of aggregates. In all samples studied herein no differences in these properties were observed (see Supporting Information).

SANS of Lysozyme in Aqueous Solution. The SANS data from lysozyme in aqueous solution are plotted on a $\log(I)$ vs q scale in Figure 1. Data from lysozyme in D_2O solution with no salt added (Figure 1a) were obtained at protein concentrations of 0.5, 1, 2, 5, 10, 20, 50, and 100 mg/mL. For the samples at concentrations of 20 mg/mL and higher, clear signs of interparticle interference, i.e., interaction between the lysozyme particles, are seen in that the data show a downturn at the lowest q values. This downturn in the data at low q allows for the observation of a broad peak in the data that is centered at approximately $q = 0.1 \text{ \AA}^{-1}$. Close examination of the 5 and 10 mg/mL data also show a slight downturn at the lowest q values. Thus, visible evidence of interparticle interference exists at concentrations of 5 mg/mL and greater when there is no salt in the solution. A more quantitative analysis was performed by fitting the data as described in the Experimental Methods section. This will be addressed later.

Data were also obtained at lysozyme concentrations of 1, 5, 10, 20, and 50 mg/mL in D_2O solutions containing 0.05 M NaCl (Figure 1b) and in 0.15 M NaCl (Figure 1c). For the 0.05 M NaCl solutions, visible evidence of interparticle interference

is observed only at concentrations of 50 mg/mL and above, and there is no visible evidence of interparticle interference up to 100 mg/mL in the 0.15 M NaCl solutions. Finally, data were obtained for 0.4 M NaCl D_2O solutions of lysozyme at 1, 5, 10, 20, and 50 mg/mL (Figure 1d). Again, there is no visible evidence of interparticle interference at any of the measured concentrations. Rather, the 50 mg/mL data show an upward slope at lower q values, which is usually an indication of the presence of higher order aggregates in the sample. Close inspection of the 20 mg/mL data shows a similar behavior at the lowest q values.

SANS of Lysozyme upon Freezing. Slow Cooling Rate.

A series of snapshots of the raw SANS data from the two-dimensional (2D) position-sensitive detector as a function of sample temperature are shown in Figure 2 for 100 mg/mL lysozyme in D_2O with 0 M NaCl. These data were obtained using the slow-cooling data collection method described in the Experimental Methods section. The corresponding one-dimensional (1D) reduced data are plotted on a $\log(I)$ vs $\log(q)$ scale in Figure 3 (based on plot from ref 31). For example, the diffuse yellow, ring-shaped scattering seen in the 20 °C 2D data (Figure 2a) corresponds to the broad peak seen in the 20 °C 1D data (red diamonds in Figure 3a). As the temperature is slowly reduced from 20 to 0 °C, the 2D data (Figure 2a–d) do not appear to change significantly. However, close inspection reveals that the diffuse yellow ring is becoming smaller in diameter. While the exact freezing point of these solutions was not determined, one should note that the freezing point of D_2O

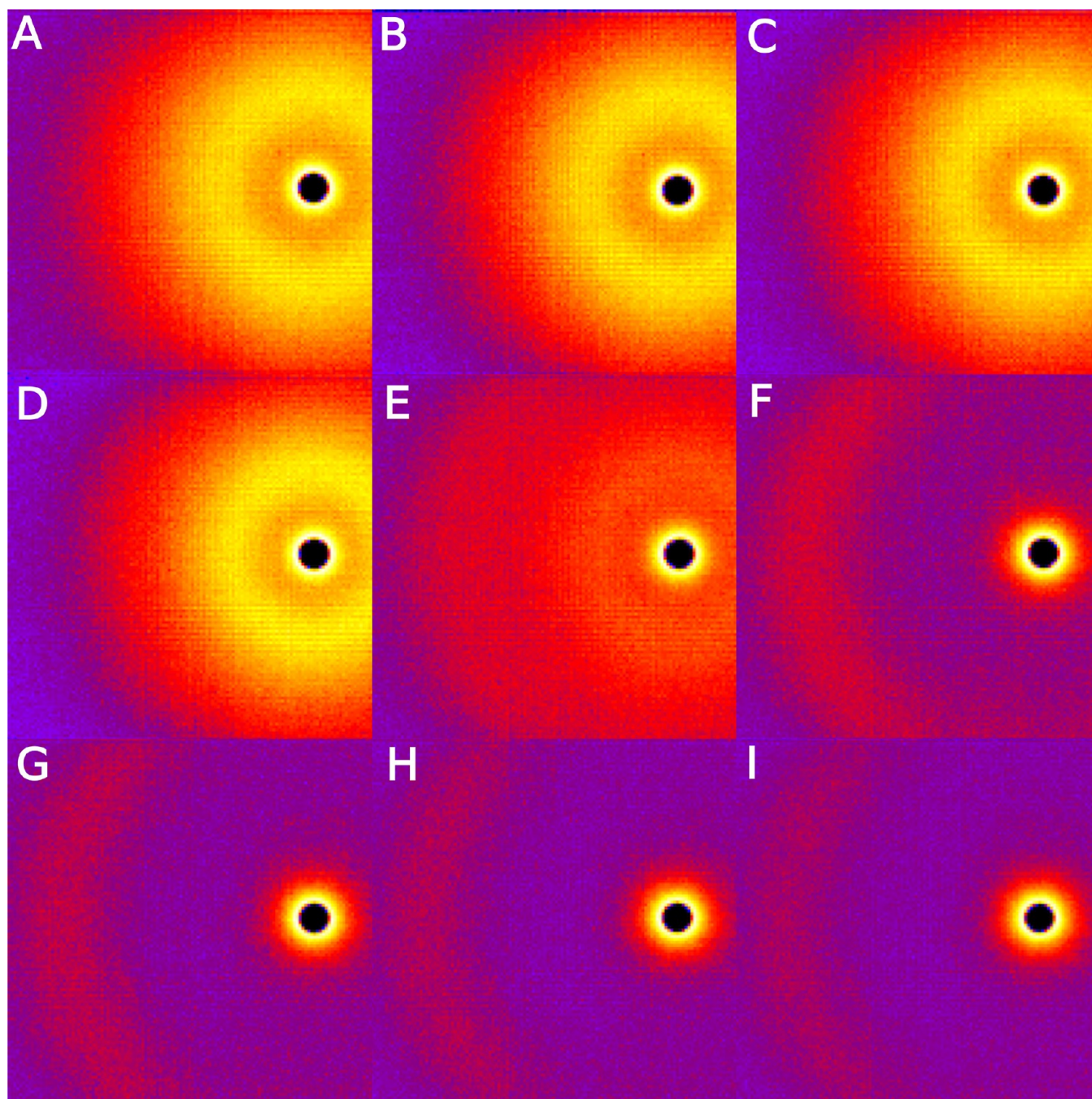


Figure 2. 2D SANS scattering profiles of lysozyme as a function of temperature obtained using a “slow cooling” protocol: (A) 20 °C, (B) 10 °C, (C) 5 °C, (D) initial scan at 0 °C, (E) intermediate scan at 0 °C, (F) final scan at 0 °C, (G) –20 °C, (H) –40 °C, and (I) –80 °C.

is 3.82 °C. The corresponding 1D data in Figure 3 show a clear shift of the broad peak in the data to lower q values (blue circles in Figure 3a). Thus, the center-to-center distance between molecules becomes slightly greater as the solution cools to 0 °C. This could be due to the formation of composite lysozyme particles as shown by SANS and neutron-spin echo spectroscopy.^{32,33} Such composite particles themselves should have a larger center-to-center distance.

As the sample sits at 0 °C, the diffuse yellow ring in the 2D data disappears (Figure 2e) and the outer part of the red area becomes more diffuse. The 1D data show a reduction of the scattered intensity as a whole as well as a shift of the broad scattering peak back to a higher q value and the appearance of

an additional peak near $q = 0.2 \text{ \AA}^{-1}$. At this point, the solution is in a mixed state, with the scattering showing evidence of lysozyme at two different concentrations (green triangles in Figure 3a).

As the sample is cooled to 0 °C, the 1D scattering of Figure 3 shows only a well-defined peak near $q = 0.2 \text{ \AA}^{-1}$, along with sharply increasing scattering at lower q values (cyan curve). The corresponding 2D scattering (Figure 2f) shows only a diffuse red partial ring on the left side of the image and a brighter red ring on the right side of the image. These two features correspond, in the 1D scattering, to the peak near $q = 0.2 \text{ \AA}^{-1}$ and the sharp increase in scattering at lower q , respectively. As the sample continues to freeze down to –80 °C, the peak near

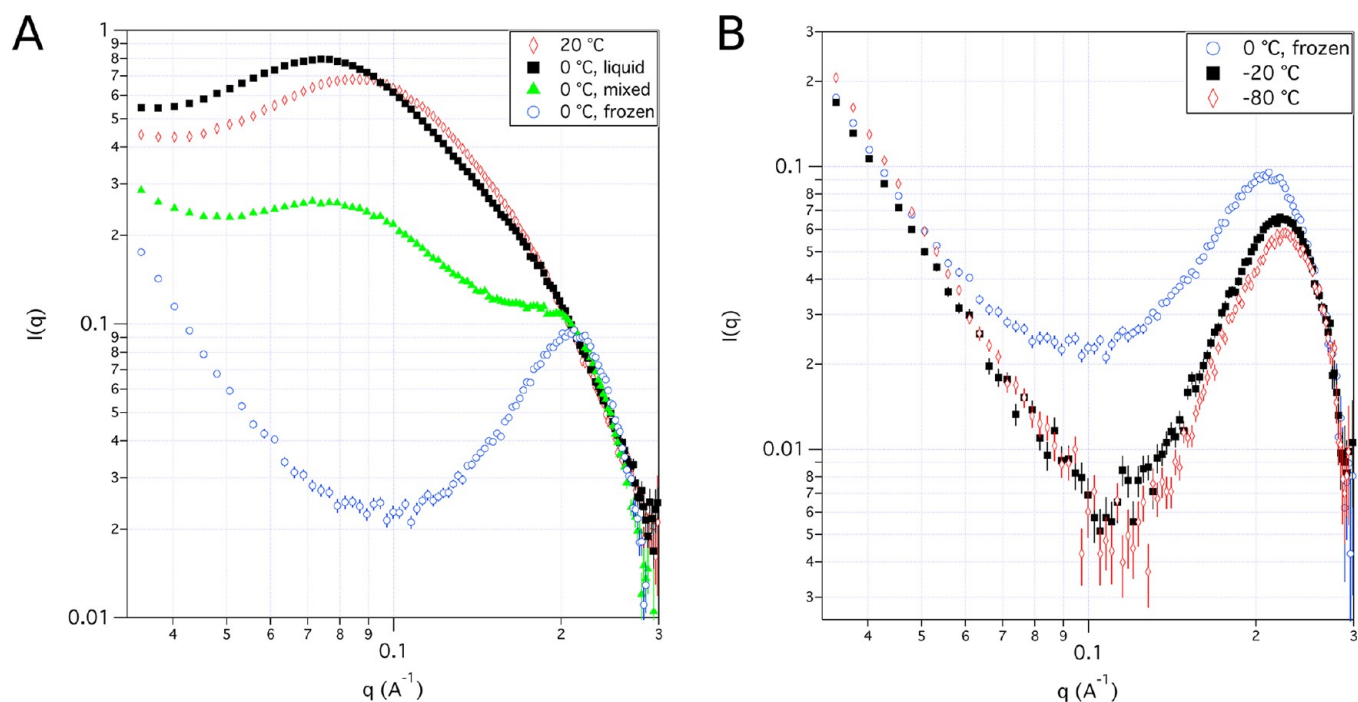


Figure 3. 1D SANS scattering profiles of lysozyme in solution as a function of temperature. (A) Liquid to frozen state and (B) frozen samples. Error bars represent ± 1 standard deviation.

$q = 0.2 \text{ \AA}^{-1}$ continues to sharpen and shift to higher q values. This can be most readily observed in the 1D data (magenta diamonds and black squares in Figure 3b), although close inspection of the 2D data (Figure 2g–i) shows a small decrease in the thickness of the partial ring and a shift toward the left side of the image, corresponding to the shift to higher q values in the 1D data.

Fast Cooling Rate. Another series of snapshots of the raw SANS data from the 2D position-sensitive detector as a function of sample temperature is shown in Figure 4 for 100 mg/mL lysozyme in D_2O with 0 M NaCl. However, these data were obtained using the “fast-cooling” data collection method described in the Experimental Methods section. Figure 4a–c shows the sample undergoing fast cooling from 20 to $-20 \text{ }^\circ\text{C}$, while Figure 4d–i shows the sample cooling under the same conditions from 20 to $-40 \text{ }^\circ\text{C}$ and 20 to $-80 \text{ }^\circ\text{C}$, respectively. While a diffuse partial ring can be seen at the left side of the images in the frozen samples (Figure 4c,f,i), the images in both Figure 4b,c,e,f,h,i are dominated by starburst features. The origin of these features is not known, but their nonisotropic nature suggests that they are due to large-scale ordering in the system upon rapid freezing, perhaps due to strain or some other process. These features could be related to cracking due to discontinuities in the stress field of the sample as has been reported for cryoprotectant solutions.³⁴ Regardless, these features dominate the low- q scattering and can interfere with the scattering from the ring feature as well, making the peak less well-defined in the 1D data. However, fast cooling does not change the location of the peak in the 1D data, as shown in Figure 5, which compares the data from 100 mg/mL lysozyme in D_2O with 0 M NaCl at $-40 \text{ }^\circ\text{C}$ obtained by both the slow cooling and fast cooling protocols. Figure 5 clearly illustrates that the “slow cooling” process results in a more well-defined peak in the 1D data. It has been shown that faster cooling rates lead to greater perturbations to native protein structure in frozen conditions⁷ and can have deleterious effects on the

manufacturing of protein products.⁵ Whether the definition shown in the “slow cooling” process is related to more segregation of lysozyme molecules or an indication of fewer unfolded (reversible) lysozyme molecules absorbed to the ice interface is not decipherable from the SANS profiles.

SANS of Lysozyme in the Frozen State. The SANS data from lysozyme in the frozen state at $-40 \text{ }^\circ\text{C}$ via the fast cooling process are plotted on a $\log(I)$ vs q scale in Figure 6. Data from frozen lysozyme in D_2O with no salt added (0 M NaCl, Figure 6a) are shown for protein concentrations of 5, 10, 20, 50, and 100 mg/mL. Similarly, data are shown from frozen lysozyme at concentrations of 5, 10, 20, 50, and 100 mg/mL in D_2O with 0.05 M NaCl (Figure 6b) and in 0.15 M NaCl (Figure 6c). Finally, data from frozen lysozyme in D_2O with 0.4 M NaCl are shown at concentrations of 5, 10, 20, and 50 mg/mL in Figure 6d. A striking feature of all of these scattering curves is the observed peak near $q = 0.2 \text{ \AA}^{-1}$. While it becomes sharper and more intense with increasing protein concentration, its location at a given temperature is independent of the initial protein concentration. Occasionally, multiple peaks were observed, as in the 10 mg/mL data obtained in D_2O with 0 M NaCl (Figure 6a).

The observed peaks in the scattering occur due to the crowding of protein as the solution freezes. As ice forms, the remaining unfrozen water becomes concentrated in a separate phase, with the amount of unfrozen water remaining at between 20 and 30 mass %.¹⁴ This solute rejection alters the local solute concentration and leads to heterogeneous microenvironments.^{7,9,10} NMR experiments³⁵ have shown that a solute-rich liquid phase persists in a solution of bovine serum albumin, potassium fluoride, and water down to temperatures as low as $-100 \text{ }^\circ\text{C}$. Furthermore, the protein concentration at subfreezing temperatures is the same regardless of the initial protein concentration prior to freezing,¹⁴ in direct agreement with the SANS data in which the position of the peak near $q = 0.2 \text{ \AA}^{-1}$ is independent of initial protein concentration.

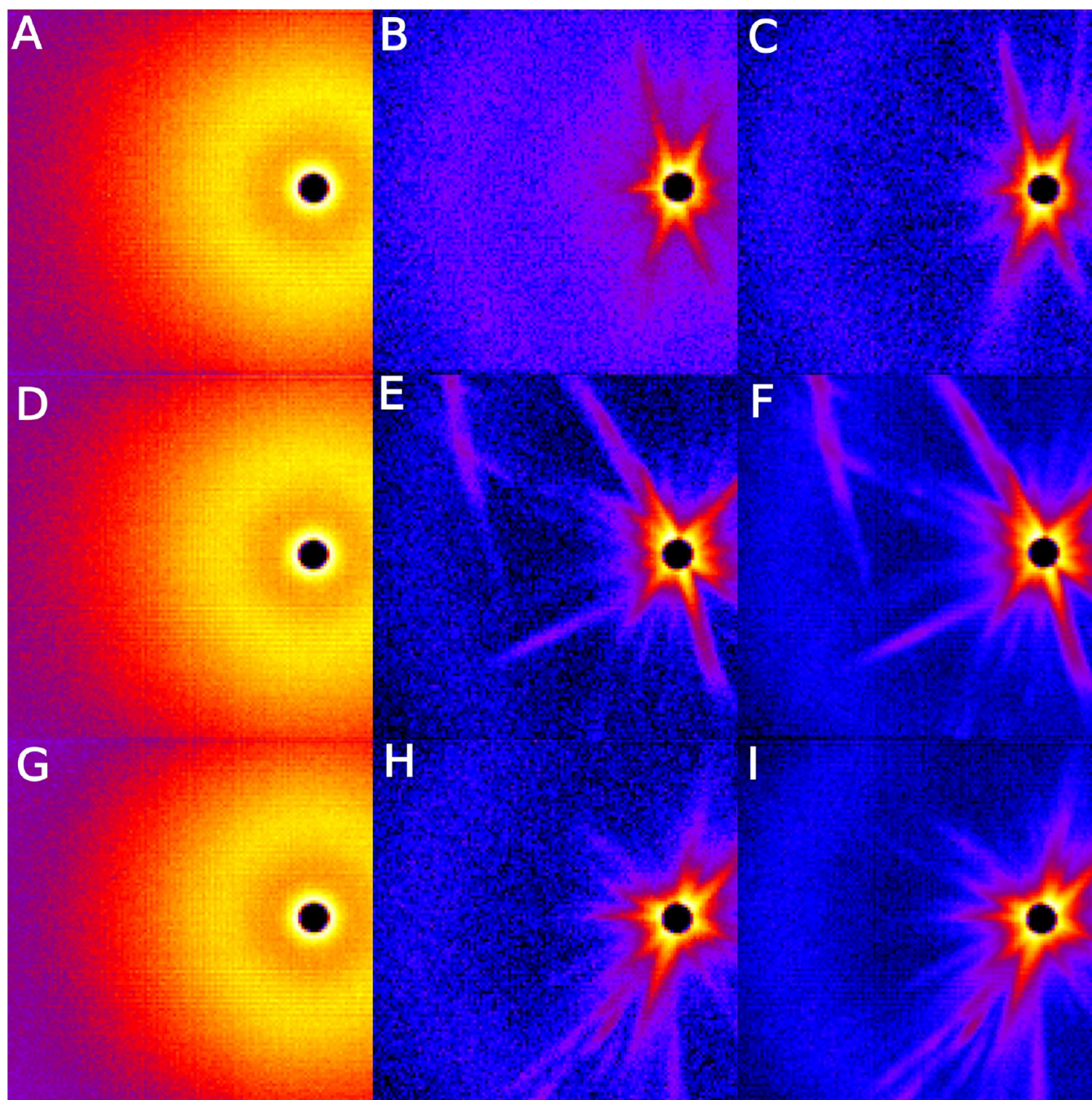


Figure 4. 2D SANS scattering profiles of lysozyme as a function of temperature obtained using a “fast cooling” protocol: (A) 20 °C, (B) cooling to −20 °C, (C) −20 °C, (D) 20 °C, (E) cooling to −40 °C, (F) −40 °C, (G) 20 °C, (H) cooling to −80 °C, and (I) −80 °C.

The low- q scattering that is evident in all of the frozen samples did not show any correlation with the initial protein concentration and could be different each time the sample was frozen. Similar low- q scattering is observed even in the absence of protein. Thus, its origin lies, at least partially, in the ice structure itself.

Contrast Series: Elucidation of Low- q Scattering. In order to ascertain whether the low- q scattering observed even in the absence of protein occurs from the contrast between air and the D₂O ice due to cracks or other similar features, a series of contrast variation experiments were performed on −40 °C frozen water solutions of several mixtures of D₂O:H₂O in the absence of protein and salt. Figure 7 shows the contrast

variation data from frozen 0, 5, 10, 20, 40, and 70% D₂O solutions on a $\log(I)$ vs $\log(q)$ scale. When the ice composition is 8% D₂O:92% H₂O, it has a neutron scattering length density of zero, which is the same as that for air. Thus, if the scattering at low q values is arising solely from the contrast between the air and ice, $\Delta\rho = 0$ (see eq 2), there should be no scattering in 8% D₂O ice. The scattering should increase as the amount of D₂O becomes larger or smaller than 8%. It can be seen from Figure 7 that this is exactly what was observed. Starting with the 0% D₂O ice scattering at the lowest q values as a reference point, the scattering is seen to decrease to essentially zero for the 5% D₂O ice, remain at zero for the 10% ice, and then increase again for the 20% D₂O ice. The intensity then

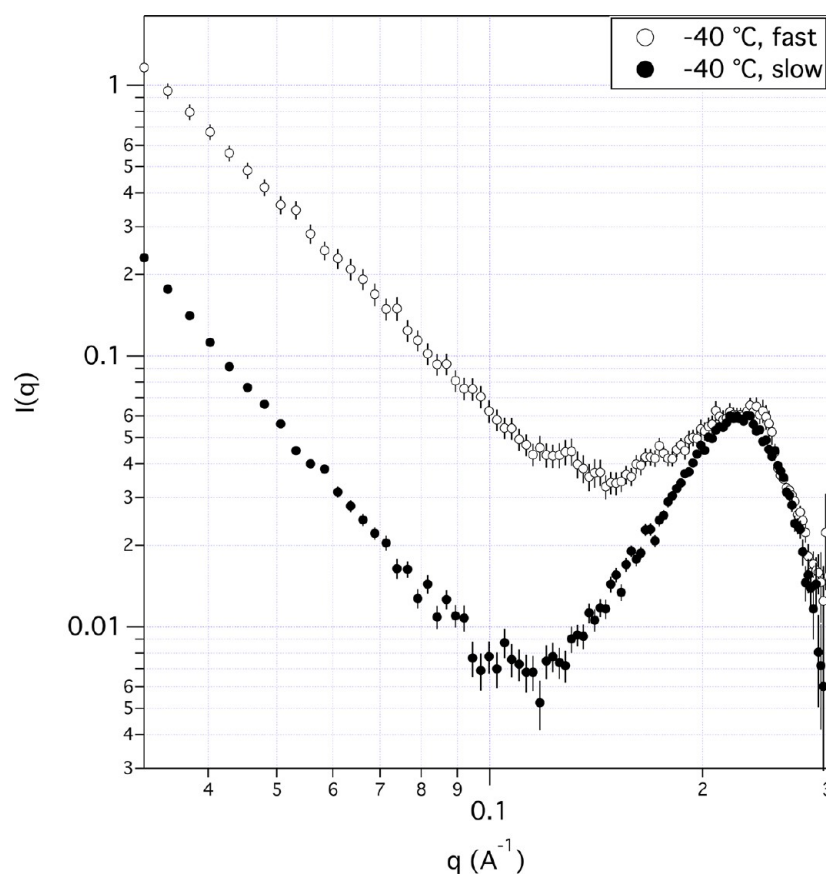


Figure 5. Comparison of freezing rates on scattering of 100 mg/mL lysozyme in D_2O and 0 M NaCl. Error bars represent ± 1 standard deviation.

continues to increase as the amount of D_2O increases. Thus, the scattered intensity is zero between 5% and 10% D_2O ice, consistent with what is expected if the scattering was due to cracks in the ice that create a contrast between air and ice. The cracks are large features, explaining why the scattering occurs mainly at lower q values.

A second contrast variation series was performed on the same frozen water solutions with 100 mg/mL lysozyme and 0 M NaCl. The data are shown on a $\log(I)$ vs $\log(q)$ scale in Figure 8. In this case, the low- q scattering does not decrease as the percentage of D_2O approaches 8%. This means that there also must be scattering from large-scale protein structures in the frozen samples that contain protein in addition to the scattering from the cracks in the ice itself. Perhaps the protein is aggregating at the boundaries of the water and ice phases in addition to being forced into tight clusters due to the small space available in the water phase. If there is some protein in the ice phase, it could propagate to the edges of the cracks formed during the freezing process, where it could form large aggregates. The structure of a solution of phosphate buffer saline (PBS) at a temperature of -26 °C has been described, using confocal Raman microscopy, as consisting of ice crystals surrounded by narrow channels and more rounded domains that contain unfrozen water.¹⁰ While protein was observed in the ice phase of PBS containing both lysozyme and trehalose, the concentration of both protein and trehalose in the unfrozen water phase was about 2 orders of magnitude greater with $\sim 1/7$ of the lysozyme observed in the ice phase. The dimensions of their heterogeneous crystalline domains are on the order of several micrometers and thus larger than the spatial scale probed by SANS. Although the scattering from these larger

structures tapers off with reducing length scale ($2\pi/q \sim 60$ Å), allowing the observation of the interaction peak in the SANS profiles in the current work.

A final contrast variation series was performed on the same frozen water solutions with 0.4 M NaCl in the absence of lysozyme. The data are shown on a $\log(I)$ vs $\log(q)$ scale in Figure 9. Once again, the low- q scattering does not decrease as the percentage of D_2O approaches 8%. This means that there also must be scattering from large-scale NaCl structures. The temperature at which these samples were measured is -40 °C: thus, in the lysozyme solutions containing salt, the salt may also be aggregating at the boundaries between the water and ice phases or at the ice–air interface. This apparent phase separation and possible precipitation of salt have been observed in desiccated protein droplets.⁹

SANS of Lysozyme in d_6 -Glucose and d -Trehalose.

Figure 10 shows the SANS data on a $\log(I)$ vs $\log(q)$ scale from 100 mg/mL lysozyme frozen at 0 °C, 100 mg/mL lysozyme freeze-dried from a 5% d_6 -glucose, and 5% d -trehalose in D_2O solutions. The scattering curves, which have been offset for clarity, look very similar, meaning that the proteins cluster in a similar manner in all three cases as water is removed from the system. The presence of an interaction peak near $q \sim 0.2$ Å⁻¹ is consistent with that found for myoglobin in a variety of saccharide matrices.³⁶ There is also significant scattering at low q in all three cases, indicating that large structures are also being measured in the system. For the case of the lysozyme in frozen D_2O , the contrast variation experiments have shown that this scattering is coming from both the protein and the ice structure itself. Since similar contrast variation experiments have not been performed on the lysozyme in the two carbohydrate

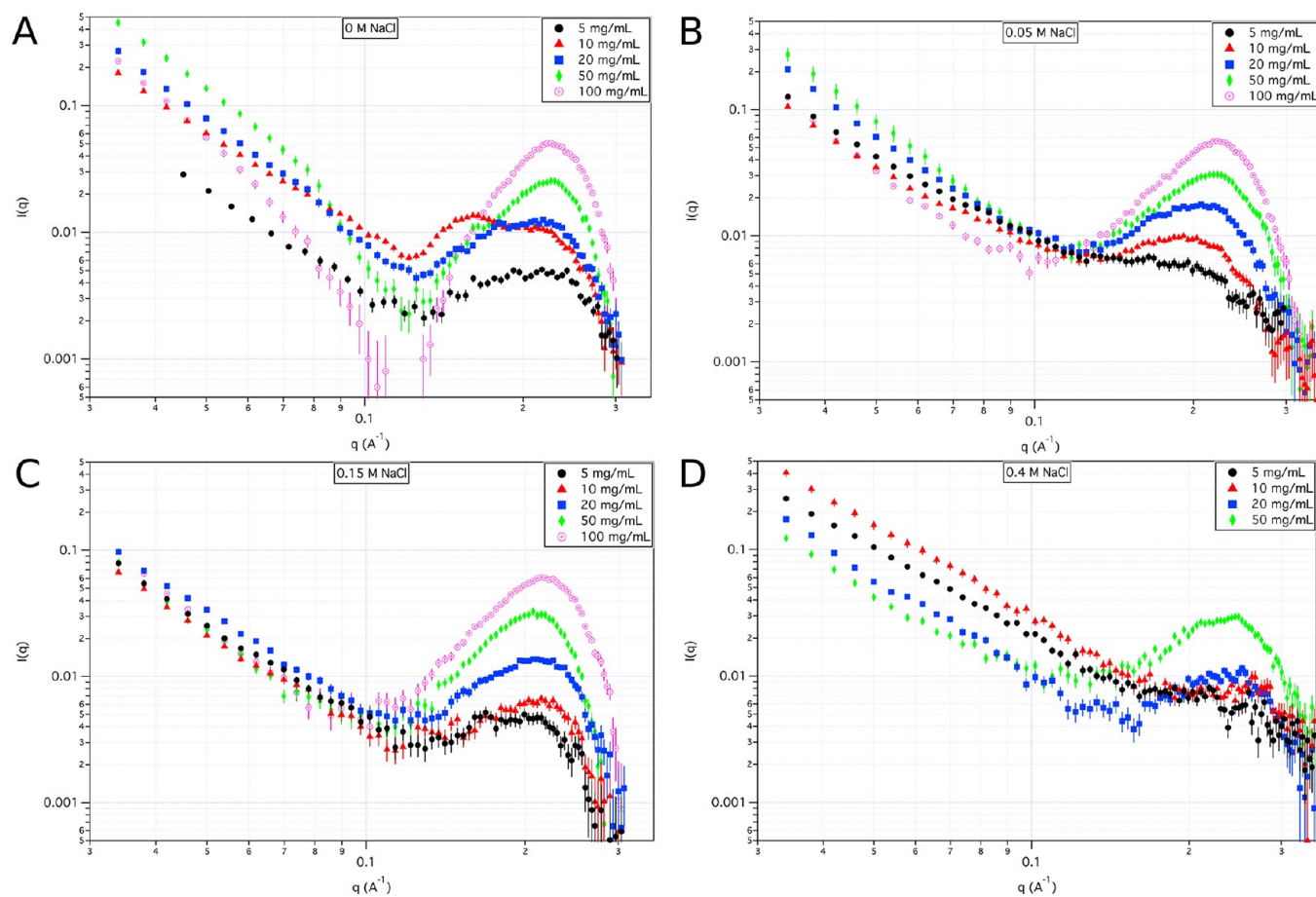


Figure 6. SANS of lysozyme in frozen solution as a function of protein and NaCl concentration: (A) 0 M NaCl, (B) 0.05 M NaCl, (C) 0.15 M NaCl, and (D) 0.4 M NaCl. Error bars represent ± 1 standard deviation.

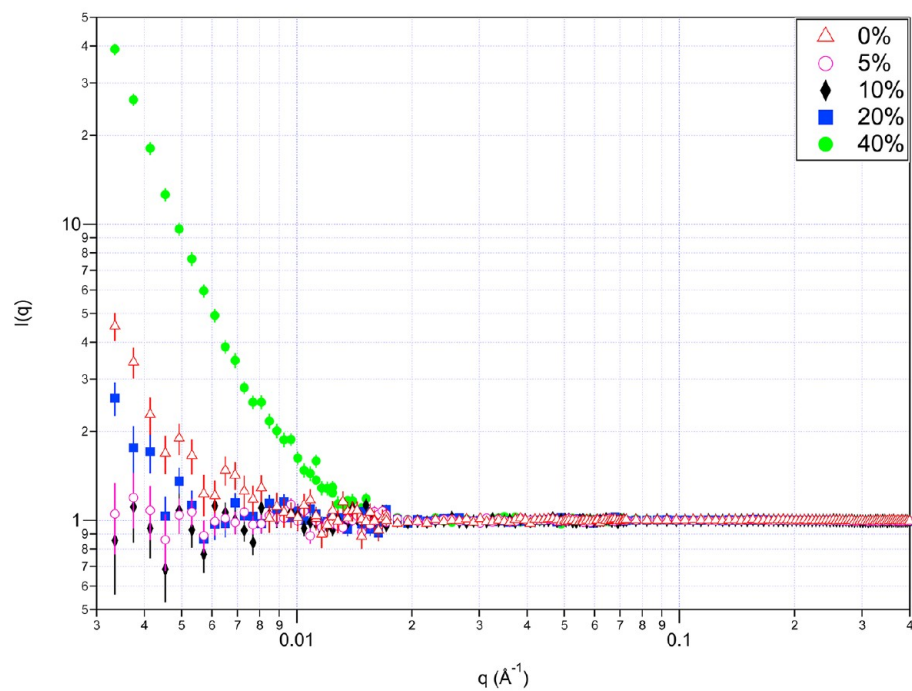


Figure 7. Contrast matching of buffer. Error bars represent ± 1 standard deviation.

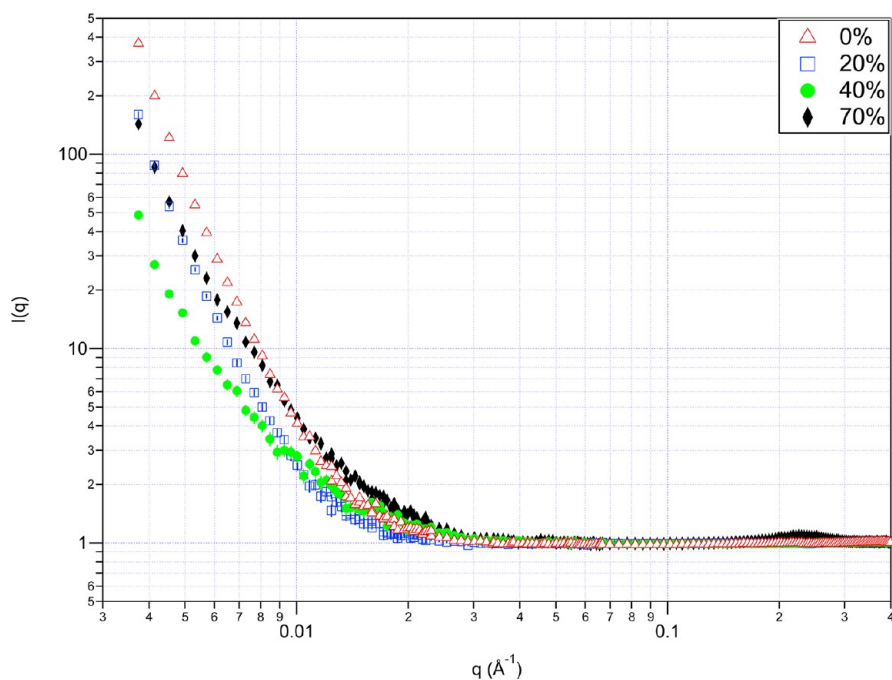


Figure 8. Contrast matching of lysozyme. Error bars represent ± 1 standard deviation.

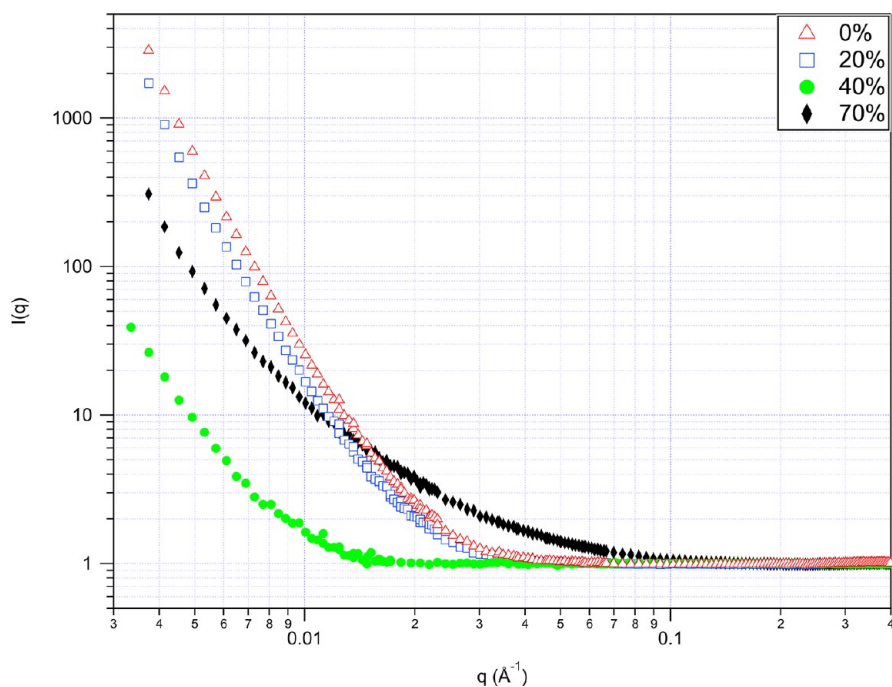


Figure 9. Contrast matching of buffer with 0.4 M NaCl. Error bars represent ± 1 standard deviation.

powders, it is not certain whether the scattering is arising from both the protein and carbohydrate structures.

Modeling of Protein–Protein Interactions. Fits were made to lysozyme at room temperature using an ellipsoidal form factor, $P(q)$, and a screened Coulomb structure factor, $S'(q)$, as described in the Experimental Methods section. The resulting best fit parameters are listed in Table S1. The length of the short axis of the ellipsoid was held fixed during the fitting process. Its value was chosen based on several fits to the 0.5 mg/mL, 0 M NaCl data, where the structure factor is assumed to be one for all q values. The best fit length of the long axis varied, for the most part, between 19 and 21 Å and was not

sensitive to the salt conditions. The best fit values were greater than 21 Å at the highest protein concentrations for the 0.05, 0.15, and 0.4 M NaCl solutions, but the χ^2 values were higher as well. The fits were only sensitive to the charge parameter for the 0 M NaCl data at concentrations at 2 mg/mL and below. Thus, the parameter was fixed for the data at the other salt conditions. The only parameter that varied significantly as a function of concentration is the volume fraction, as expected.

The $\log(I)$ vs $\log(q)$ room temperature data as a function of lysozyme concentration are shown in Figure 11a,b for the 0 M NaCl and 0.4 M NaCl samples. The solid lines are representative fits to the data for selected concentrations. The

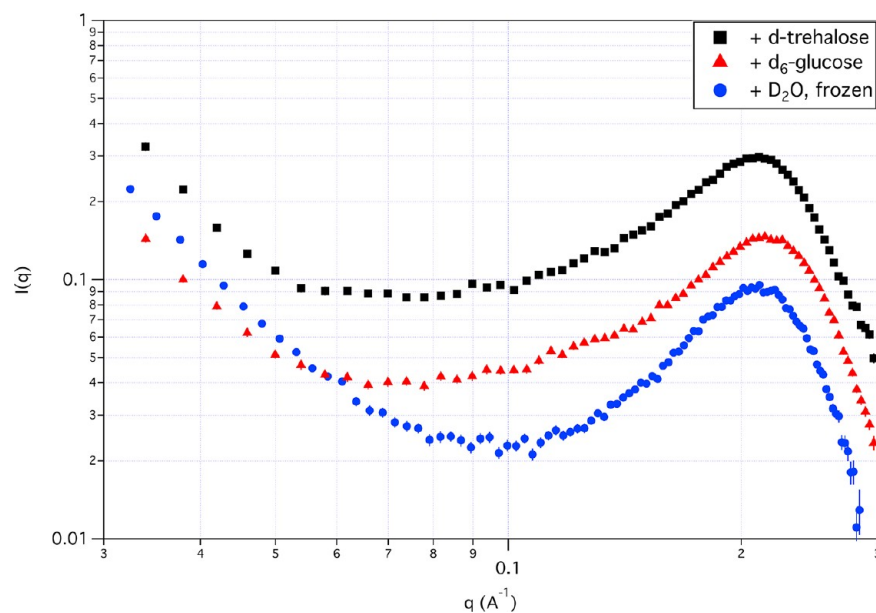


Figure 10. SANS of lysozyme in various solid states. Error bars represent ± 1 standard deviation.

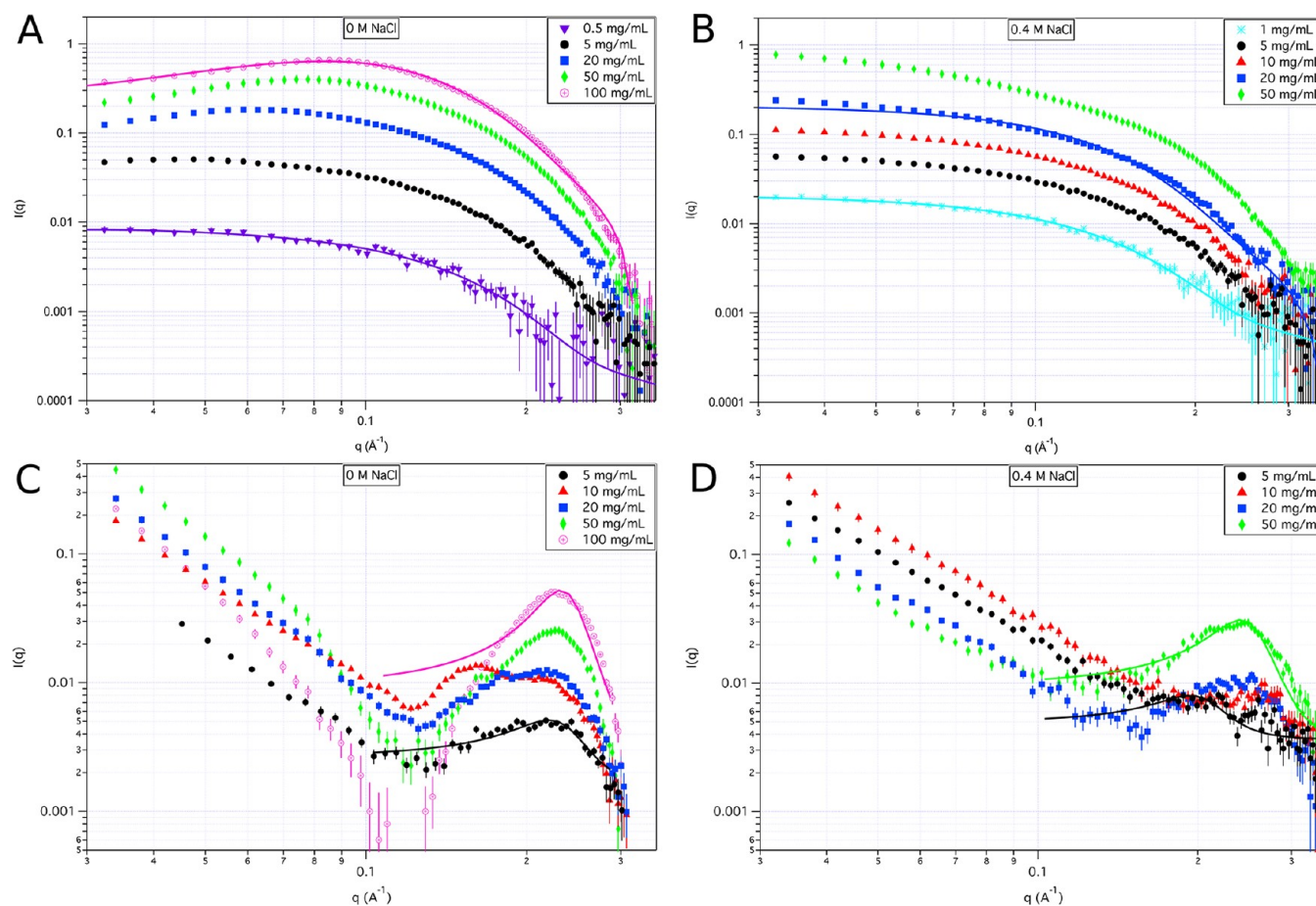


Figure 11. Screened Coulomb and hard-sphere fitting: (A) 0 M NaCl, (B) 0.05 M NaCl, (C) 0.15 M NaCl, and (D) 0.4 M NaCl. Solid lines are representative fitting results (see text for further information). Error bars represent ± 1 standard deviation.

fitted lines match the data well up to 100 mg/mL for the 0 M NaCl data. However, the fit already deviates significantly from the data at 20 mg/mL for the 0.4 M NaCl condition. This implies that the model used to fit the 0.4 M NaCl data does not describe the data well at higher concentrations. This is also

apparent from Table S1, where the best fit χ^2 values at the higher concentrations are significantly higher for the data with 0.05 M NaCl, 0.15 M NaCl, and 0.4 M NaCl than for the 0 M NaCl data. It is likely that there is polydispersity in the system once salt is introduced, as the salt screens the charge on the

proteins, weakening the electrostatic repulsion in the system and allowing the proteins to form aggregates more easily most likely due to a relative enhancement of hydrophobic interactions.³⁷ Thus, a size distribution of protein monomers and lower order oligomers, such as dimers, trimers, etc., can coexist in solution. However, the fitting function assumes a monodisperse solution of ellipsoidal particles, so the fits are not as good as the concentration of salt in the solution increases.

The $\log(I)$ vs $\log(q)$ frozen lysozyme data (-40 °C) as a function of lysozyme concentration are shown in Figure 11c,d for the 0 and 0.4 M NaCl samples. The solid lines are representative fits to the higher q portion of the data for selected concentrations. No attempt was made to subtract the scattering at lower q values due to the nonreproducible nature of that portion of the scattering curve upon freezing. The fits were made using an ellipsoidal form factor, $P(q)$, and a hard-sphere structure factor, $S'(q)$, as described in the Experimental Methods section. A screened Coulomb structure factor was also used in a few cases for comparison. The fitted lines match the data best at the lower concentrations, where the peak is not as sharp and the goodness of fit does not depend on the salt concentration. The χ^2 values for the higher concentration data could be significantly influenced by the range of data points chosen.

The resulting best fit parameters are listed in Table S2. Again, the length of the short axis of the ellipsoid was held fixed during the fitting process to the same value that was used for the room temperature data. The best fit length of the long axis is shown for both the liquid and frozen states as a function of protein concentration in Figure 12 for the samples with varying

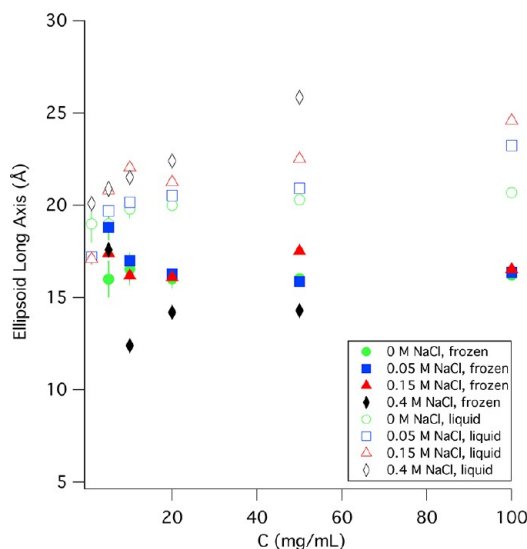


Figure 12. Lysozyme model ellipsoid long dimension as a function of concentration in both liquid and frozen states. Error bars represent ± 1 standard deviation.

salt concentration. This parameter was systematically smaller for the samples in the frozen state than for the samples in the liquid state. It can be seen from Figure 11 that the values for the frozen samples varied, for the most part, between 15 and 18 Å, compared to between 19 and 21 Å for the liquid state samples. The best fit length of the long axis was even smaller, i.e., between 12 than 14 Å for the 0.4 M NaCl data at concentrations above 5 mg/mL. In the cases where multiple peaks were observed, the value from fits to the peak

representing the second population was 23 Å, as shown in Table S2.

The volume fraction of lysozyme in both the liquid and frozen states is plotted as a function of protein concentration in Figure 13. The volume fraction of lysozyme in the liquid state

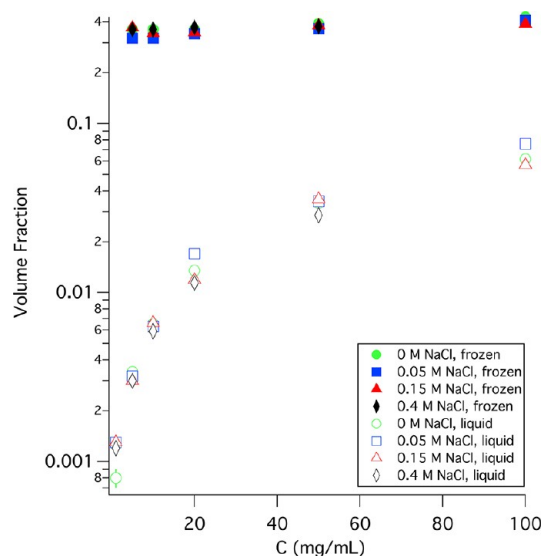


Figure 13. Volume fraction of lysozyme as a function of concentration in both liquid and frozen states. Error bars represent ± 1 standard deviation and are smaller than the points depicted used represent the data.

varied strongly with protein concentration, as expected since the proteins are being forced closer together as the concentration increases. However, the volume fraction did not vary systematically with salt concentration. The lowest value was 0.000 54 for the 0.5 mg/mL 0 M NaCl sample, and the highest value was 0.076 for the 100 mg/mL 0.05 M NaCl sample. On the other hand, the volume fraction of frozen lysozyme varied between 0.32 and 0.43 and did not strongly depend on the initial protein or salt concentrations in the solid phase. Differences seen in Figure 13 are more likely due to differences in temperature, which varied between the range of -35 and -45 °C during the experiment, as the location of the interaction peak depends strongly on the temperature of the sample.

Finally, fits to the data could not be achieved if the solvent scattering length density (SLD) was held fixed at the value for D_2O . Rather, the solvent SLD was allowed to vary during the fitting procedure, resulting in best fit values between 3.2×10^{-6} and $3.9 \times 10^{-6} \text{ \AA}^{-2}$, and showed no obvious dependence on salt concentration. However, in this case, the solvent is a mixture of both unfrozen water and ice, which in addition contains air pockets or cracks that form during the freezing process. Since these air pockets have a SLD of zero, this reduces the overall SLD of the solvent.

The slow cooling temperature series data were also fit using an ellipsoidal form factor, $P(q)$, and a hard-sphere structure factor, $S'(q)$, as described in the Experimental Methods section. The resulting best-fit parameters from the 0 M NaCl lysozyme sample cooled from 20 to -80 °C are listed in Table 1. The temperature was carefully controlled during the cooling process, and the sample was allowed to equilibrate at each temperature. Thus, the observed change in volume fraction is a reliable parameter for describing the crowding of the protein

Table 1. Fitting Parameters for 100 mg/mL Lysozyme with 0 M NaCl Using an Ellipsoidal Form Factor and Hard-Sphere and/or Screened Coulomb Structure Factor^a

temp (°C)	vol fraction	a (Å)	b (Å)	solvent SLD (10^{-6} \AA^{-2})	charge (SC only)	χ^2
20.00 ± 0.05	0.0659 ± 0.0001	9	21.10 ± 0.1	6.4	4.70 ± 0.02	6.2
0.00 ± 0.05	0.0583 ± 0.0001	9	23.32 ± 0.02	6.4	4.18 ± 0.02	10.4
0.00 ± 0.05	0.19	9	19.69 ± 0.05	6.540 ± 0.006	6.3 ± 0.1	1.2
0.00 ± 0.05*	0.23	9	15.72 ± 0.03	4.505 ± 0.002		1.4
0.00 ± 0.05	0.381 ± 0.001	9	17.01 ± 0.03	4.128 ± 0.002		3.5
-20.00 ± 0.05	0.409 ± 0.002	9	16.41 ± 0.04	3.954 ± 0.003		3.5
-80.00 ± 0.05	0.426 ± 0.002	9	16.44 ± 0.04	3.880 ± 0.003		4.6

^aSolvent SLD was held fixed for liquid state and allowed to vary for mixed and frozen states. Protein SLD was fixed at $3.0 \times 10^{-6} \text{ \AA}^{-2}$. Dielectric constant was fixed at 80 for screened Coulomb (SC) structure factor. Parameters without errors listed were held fixed. Errors represent one standard deviation of statistical uncertainty of the fitting parameters (* indicates a second population).

during the freezing process. A plot of the volume fraction as a function of temperature is shown in Figure 14. The main

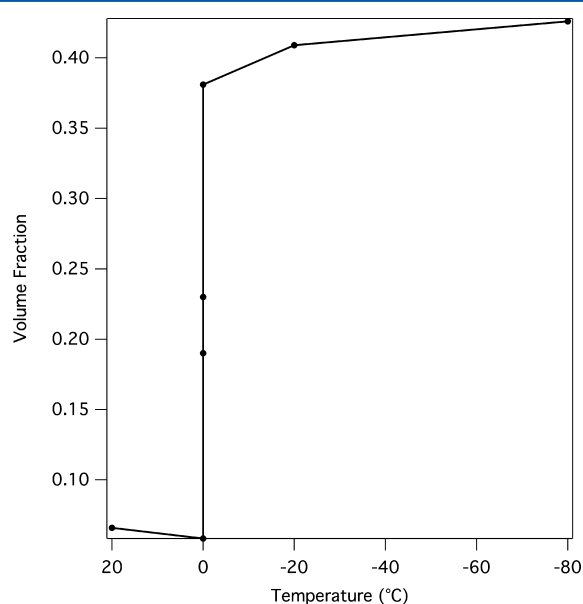


Figure 14. Volume fraction of 100 mg/mL lysozyme in 0 M NaCl as a function of temperature. Error bars represent ± 1 standard deviation.

feature is the sharp increase in volume fraction as the sample freezes at 0 °C. The volume fraction continues to increase with decreasing temperature all the way down to -80 °C.

Monte Carlo Simulations of Lysozyme Configurations in Liquid and Solid Phases.

The fitting procedure used above gives some insight into the changes that occur in the lysozyme solution as a function of initial concentration and temperature. However, it clearly has limitations since most proteins, including lysozyme, are not well modeled by simple geometric shapes. A complete atomistic representation to model frozen states including counterions and the known microheterogeneity is a challenging task. Our approach is to use a simple model in order to visualize the real-space arrangement of lysozyme particles in order to reconcile the current observations and interpretation of SANS measurements with pre-existing descriptions and observations of proteins in frozen samples. In Figure 15, typical snapshots of lysozyme particles at volume fractions corresponding the initial 100 mg/mL solution at 25 and -80 °C are shown. One can see that at -80 °C there is a distribution of interprotein distances and a significant free-volume that in real samples can be occupied by water, ions, and cryoprotectants. We are extending our computational approaches to model such heterogeneous systems.

CONCLUSIONS

This work has shown that protein structure and interactions can be monitored during the freezing process using SANS. Qualitative changes in volume fraction as a function of temperature and salt concentration can be readily observed. These changes were found to be unaffected by the rate of cooling, although faster cooling resulted in an overall deformation of the sample on a length scale larger than that readily measured with SANS, i.e., micrometers or larger. The

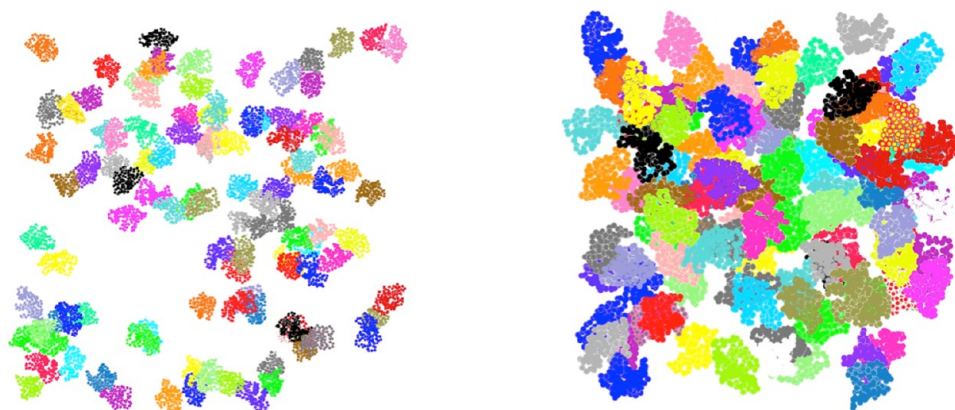


Figure 15. Results of Monte Carlo simulation of lysozyme at 100 mg/mL with 0 M NaCl in the liquid and frozen states. From left to right, $\eta \sim 0.068$: 25 °C and $\eta \sim 0.36$: -80 °C (not depicted on the same scale).

SANS data were fit using an ellipsoidal form factor and either a screened-Coulomb or hard-sphere interaction potential in order to obtain quantitative information on the change in lysozyme volume fraction as a function of temperature and salt concentration. The expected change in volume fraction during the freezing process is observed, including the initial decrease in volume fraction as the water expanded prior to freezing, followed by a rapid increase in volume fraction as the solution freezes and a continued slow increase in volume fraction as the temperature is further decreased to $-80\text{ }^{\circ}\text{C}$. Salt had little effect on the volume fraction of the frozen sample.

The change in shape of lysozyme as a function of temperature and salt concentration was monitored by observing the change in the fitted long dimension of the ellipsoid, while holding the short dimensions fixed during the fitting procedure. A decrease in this parameter was observed both with increasing salt concentration and decreasing temperature. The difference in shape cannot be strictly associated with the protein length, since the length and width are coupled in the fitting procedure and the width was held fixed in order to have a reasonable reference point for comparison of the fits to all of the data. However, the decrease in the overall fitted size of lysozyme suggests that it does not radically denature upon freezing or in high salt conditions. Regardless, changes in secondary structure^{7–10} and tertiary structure^{7,8} have been reported for several proteins in water–ice. Taken together, the SANS data reported here and pre-existing fluorescence, infrared, and Raman studies indicate that the structural changes of protein absorbed to water–ice does not involve large changes in the aspect ratio of a large fraction of the protein molecules in the sample. Although these initial results are promising, a systematic study of lysozyme and other proteins in the presence of different salts, sugars (stabilizers), and denaturants (destabilizers) are necessary in order to determine whether the fitting method used reliably reports changes in protein shape upon freezing. Advancements in simulation methods to accurately capture the association and conformational changes of proteins at water–ice surfaces and similar heterogeneous phases are needed to model the observed changes in SANS profiles.

Contrast variation experiments made it possible to determine that the low- q scattering observed in the frozen 0 M NaCl D_2O solution is due to the contrast between water and the air that is present in the ice matrix due to cracks that form upon freezing. When salt is present in the frozen solution, it also contributes to the low- q scattering, meaning that there are large aggregates of salt present in the frozen salt solutions. Similarly, when lysozyme is present in the frozen solution in the absence of salt, it also contributes to the low- q scattering, meaning that there are large aggregates of lysozyme present, in addition to clusters of densely packed protein, as evidenced by the peak in the scattering curves near $q = 0.2\text{ }\text{\AA}^{-1}$. For all conditions tested, these aggregates were not found upon thawing of the samples. Based on the information obtained from the SANS contrast variation data of the 100 mg/mL lysozyme solution with 0 M NaCl and the Monte Carlo simulations of the same system, along with information obtained by others using Raman scattering¹⁰ and NMR,³⁵ as well as a basic knowledge of the behavior of water upon freezing,¹⁴ a cartoon of the morphology of the sample in the frozen state has been constructed as shown in Figure 16.

As drawn in the figure, the frozen state consists mainly of ice crystals, with regions of amorphous water containing freeze-

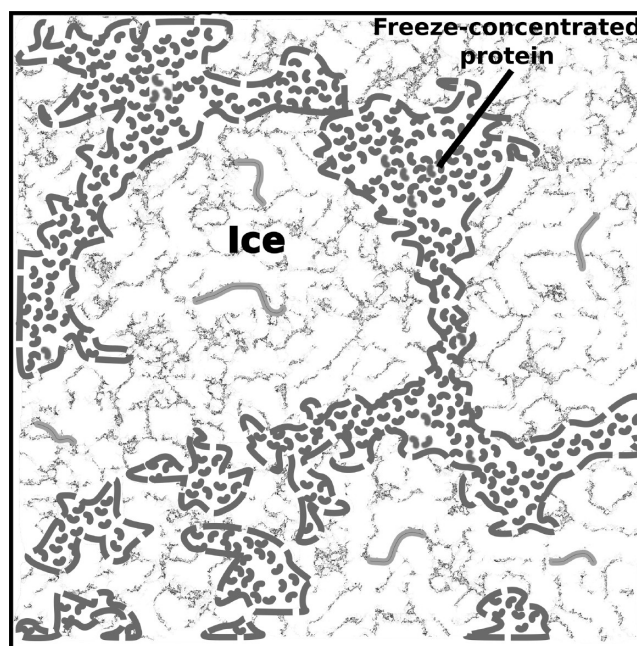


Figure 16. Cartoon of the morphology of 100 mg/mL lysozyme in 0 M NaCl D_2O solution at $-40\text{ }^{\circ}\text{C}$ (based partly on Dong et al.¹⁰). The ice and freeze-concentrated protein phases are labeled. The dark gray lines represent large protein aggregates at the boundary between the ice and freeze-concentrated protein regions. The lighter gray lines in the ice phase represent possible protein aggregates trapped at the ice–air interface. Dimensions of the freeze-concentrated proteins and protein aggregates are enlarged for clarity.

concentrated protein. It is speculated that the protein aggregates that contribute to the low- q scattering in the SANS curves form at either the ice–water or ice–air interfaces. The Raman results showed that the majority of the protein exists in the amorphous water phase.¹⁰ Thus, while some of the protein aggregates may be trapped in the ice phase at the ice–air interface, the majority of the protein is drawn to be at the ice–water interface in the figure. The remaining protein is shown to exist as close-packed monomers in the unfrozen amorphous water region, as indicated by the higher q scattering in the SANS curves. It is clear from the Monte Carlo simulations that the volume fraction obtained from the fits to the SANS data represents an average and that there is a range of distances at which the molecules are packed for any given volume fraction.

It is well-known that saccharides have cryoprotectant properties and the distribution of saccharides in frozen ternary protein containing systems has been reported.^{9,10} It is interesting that the relative interprotein distance and distribution of distances is very similar for proteins in water–ice and hydrated glucose, trehalose, and, as previously reported, other saccharides.³⁶ Knowing that a common volume fraction exists that is independent of starting concentration or medium can be advantageous in the design of both experimental and computational approaches to understand the microscopic details of protein interactions and stabilities in such environments.

■ ASSOCIATED CONTENT

■ Supporting Information

Details of the data fitting functions as well as tables with the best fit parameters. This material is available free of charge via the Internet at <http://pubs.acs.org>.

■ AUTHOR INFORMATION

Corresponding Author

*E-mail joseph.curtis@nist.gov (J.E.C.), susan.krueger@nist.gov (S.K.); Ph 301-975-3959, 301-975-6734; Fax 301-921-9847.

Notes

The authors declare no competing financial interest.

■ ACKNOWLEDGMENTS

This work utilized facilities supported in part by the National Science Foundation under Agreement DMR-0944772. S. Khodadadi acknowledges funding from the National Research Council.

■ REFERENCES

- (1) Chi, E. Y.; Krishnan, S.; Randolph, T. W.; Carpenter, J. F. *Pharm. Res.* **2003**, *20*, 1325–1336.
- (2) Arakawa, T.; Kita, Y.; Carpenter, J. F. *Pharm. Res.* **1991**, *8*, 285–291.
- (3) Carpenter, J. F.; Pikal, M. J.; Chang, B. S.; Randolph, T. W. *Pharm. Res.* **1997**, *14*, 969–975.
- (4) Chang, B. S.; Beauvais, R. M.; Dong, A.; Carpenter, J. F. *Arch. Biochem. Biophys.* **1996**, *331*, 249–258.
- (5) Rathore, N.; Rajan, R. S. *Biotechnol. Prog.* **2008**, *24*, 504–514.
- (6) López-Dóeza, E. C.; Boneb, S. *Biochem. Biophys. Acta* **2004**, *1673*, 139–148.
- (7) Strambini, G. B.; Gabellieri, E. *Biophys. J.* **1996**, *70*, 971–976.
- (8) Strambini, G. B.; Gonnelli, M. *Biophys. J.* **2007**, *92*, 2131–2138.
- (9) Ragoonanan, V.; Aksan, A. *Biophys. J.* **2008**, *94*, 2212–2227.
- (10) Dong, J.; Hubel, A.; Bischof, J. C.; Aksan, A. *J. Phys. Chem. B* **2009**, *113*, 10081–10087.
- (11) Soyer, A.; Özalp, B.; Dalmis, U.; Bilgen, V. *Food Chem.* **2010**, *120*, 1025–1030.
- (12) Rahman, M. S. *Trends Food Sci. Technol.* **2006**, *17*, 129–141.
- (13) Franks, F. *Pure Appl. Chem.* **1997**, *69*, 915–920.
- (14) Franks, F. *Biophysics and Biochemistry at Low Temperatures*; Cambridge University Press: New York, 1985.
- (15) Gabellieri, E.; Stambini, G. B. *Biophys. J.* **2003**, *85*, 3214–3220.
- (16) Babu, C. R.; Hilser, V. J.; Wand, A. J. *Nat. Struct. Mol. Biol.* **2004**, *11*, 352–357.
- (17) Kuelto, L. A.; Wang, W.; Randolph, T. W.; Carpenter, J. F. *J. Pharm. Sci.* **2008**, *97*, 1801–1812.
- (18) Smith, J. C. *Q. Rev. Biophys.* **1991**, *24*, 227–291.
- (19) Gabel, F.; Bicout, D.; Lehnert, U.; Tehei, M.; Weik, M.; Zaccai, G. *Q. Rev. Biophys.* **2002**, *35*, 327–367.
- (20) Frolich, A.; Gabel, F.; Jasnin, M.; Lehnert, U.; Oesterhelt, D.; Stadler, A. M.; Tehei, M.; Weik, M.; Wood, K.; Zaccai, G. *Faraday Discuss.* **2009**, *141*, 117–130.
- (21) Caliskan, G.; Mechtani, D.; Roh, J. H.; Kisliuk, A.; Sokolov, A. P.; Azzam, S.; Cicerone, M. T.; Lin-Gibson, S.; Peral, I. *J. Chem. Phys.* **2004**, *121*, 1978–1983.
- (22) Glinka, C. J.; Barker, J. G.; Hammouda, B.; Krueger, S.; Moyer, J. J.; Orts, W. J. *J. Appl. Crystallogr.* **1998**, *31*, 430–445.
- (23) Kline, S. R. *J. Appl. Crystallogr.* **2006**, *39*, 895–900.
- (24) Hansen, J. P.; Hayter, J. B. *Mol. Phys.* **1982**, *46*, 651–656.
- (25) Hayter, J. B.; Penfold, J. *Mol. Phys.* **1981**, *42*, 109–118.
- (26) Perkus, J. K.; Yevick, G. *J. Phys. Rev.* **1958**, *110*, 1–13.
- (27) McDonald, I. R. *Chem. Phys. Lett.* **1969**, *3*, 241–243.
- (28) Allen, M. P.; Tildesley, D. J. *Computer Simulation of Liquids*; Clarendon Press: Oxford, 1987.

(29) Cardinaux, F.; Stradner, A.; Schurtenberger, P.; Sciortino, F.; Zaccarelli, E. *Eur. Phys. Lett.* **2007**, *77*, 48004.

(30) Diamond, R. *J. Mol. Biol.* **1974**, *82*, 371–391.

(31) Curtis, J. E.; McAuley, A.; Nanda, H.; Krueger, S. *Faraday Discuss.* **2012**, DOI: 10.1039/c2fd20027a.

(32) Porcar, L.; Falus, P.; Chen, W.-R.; Faraone, A.; Fratini, E.; Hong, K.; Baglioni, P.; Liu, Y. *J. Phys. Chem. Lett.* **2009**, *1*, 126–129.

(33) Liu, Y.; Porcar, L.; Chen, J.; Chen, W.-R.; Falus, P.; Faraone, A.; Fratini, E.; Hong, K.; Baglioni, P. *J. Phys. Chem. B* **2010**, *115*, 7238–7247.

(34) Rabin, Y.; Steif, P. S.; Hess, K. C.; Jimenez-Rios, J. L.; Palastro, M. C. *Cryobiology* **2006**, *53*, 75–95.

(35) Ramirez, J. E.; Cavanaugh, J. R.; Purcell, J. M. *J. Phys. Chem.* **1974**, 807–810.

(36) Giuffrida, S.; Panzica, M.; Giordano, F. M.; Longo, A. *Eur. Phys. J. E* **2011**, *34*, 87.

(37) Curtis, R. A.; Ulrich, J.; Montaser, A.; Prausnitz, J. M.; Blanch, H. W. *Biotechnol. Bioeng.* **2002**, *79*, 367–380.